nature materials

ARTICLES

https://doi.org/10.1038/s41563-020-0798-1

Check for updates

Mechanically robust lattices inspired by deep-sea glass sponges

Matheus C. Fernandes[1,2], Joanna Aizenberg[1,2,3], James C. Weaver[1,2]✉ and Katia Bertoldi[1,2,3]✉

The predominantly deep-sea hexactinellid sponges are known for their ability to construct remarkably complex skeletons from amorphous hydrated silica. The skeletal system of one such species of sponge, *Euplectella aspergillum*, consists of a square-grid-like architecture overlaid with a double set of diagonal bracings, creating a chequerboard-like pattern of open and closed cells. Here, using a combination of finite element simulations and mechanical tests on 3D-printed specimens of different lattice geometries, we show that the sponge's diagonal reinforcement strategy achieves the highest buckling resistance for a given amount of material. Furthermore, using an evolutionary optimization algorithm, we show that our sponge-inspired lattice geometry approaches the optimum material distribution for the design space considered. Our results demonstrate that lessons learned from the study of sponge skeletal systems can be exploited for the realization of square lattice geometries that are geometrically optimized to avoid global structural buckling, with implications for improved material use in modern infrastructural applications.

The mineralized skeletal system of the hexactinellid sponge, *Euplectella aspergillum*, commonly known as the Venus' flower basket, has received considerable attention from the engineering and materials science communities for its remarkable hierarchical architecture and mechanical robustness across multiple length scales. Its constituent glassy skeletal elements (spicules) consist of a central proteinaceous core surrounded by alternating concentric layers of consolidated silica nanoparticles and thin organic interlayers[1–3]. These spicules are further organized to form a highly regular square grid, reinforced by two intersecting sets of paired diagonal struts, creating a chequerboard-like pattern of alternating open and closed cells (Fig. 1). Although the effects of the spicules' laminated architecture in retarding crack propagation[4] and increasing buckling strength[5] have been demonstrated previously, the potential mechanical benefits of the double-diagonal square lattice created from the assembly of these constituent spicules remain largely unexplored.

Grid-like open-cell lattices, such as those found in the skeletal system of *E. aspergillum*, are commonly employed in engineering contexts owing to their reduced weight[6,7], high energy absorption[8] and ability to control the propagation of acoustic[9] and thermal waves[10–12]. Generally, the properties and functionality of such geometries are dictated by their node connectivity. For example, a minimum node connectivity of six is required for two-dimensional lattices to be stretching-dominated, and thereby achieve a higher strength-to-weight ratio for structural applications[13]. In contrast, lattices with simple square geometries (with a node connectivity of four), are unstable when the loading vector has a transverse component (they are bending-dominated, and the only shear resistance arises from the joints)[14], and typically require diagonal bracing for stabilization[15].

Here we use the skeletal anatomy of *E. aspergillum* as inspiration for the design of mechanically robust square lattice architectures (more information on the skeletal structure of the sponge can be found in Supplementary Section 1 and Supplementary Fig. 1). First, we use a combination of experimental and numerical analyses to investigate the mechanical properties of the sponge's skeletal lattice. We then employ an optimization algorithm to identify the beam configuration in a diagonally reinforced square lattice that achieves the highest critical load, revealing—unexpectedly—that the skeletal system of *E. aspergillum* is very close to this design optimum. These results demonstrate that an integrated work flow, combining biological, computational and mechanical testing approaches, can guide the design of lattice architectures that are structurally more robust than those now employed in modern infrastructure and devices.

To understand the mechanical benefits of the sponge's skeletal architecture, we compared the performance of its geometry to that of three other 2D square-base lattices, all with the same total volume (that is, the same total amount of material) to ensure a fair comparison[14]. In each of these structures, the base square architecture was comprised of elements with lengths L, and with rectangular cross-sections characterized by a depth H that is large enough to avoid out-of-plane deformation. More specifically, we considered Design A, which was inspired by the sponge and comprised horizontal and vertical (non-diagonal) elements with thickness $T_{A,nd}=0.1L$ and two sets of parallel double diagonals with thickness $T_{A,d}=0.05L$ located at a distance $S=L/(\sqrt{2}+2)$ from the nodes (Fig. 2a); Design B, which was similar to the sponge-inspired design with $T_{B,nd}=0.1L$, but only contained a single diagonal with thickness $T_{B,d}=0.1L$ crossing each of the closed cells (Fig. 2b); Design C, which was inspired by the bracings found in modern engineering applications with $T_{C,nd}=0.1L$ and contained a crossed set of diagonal beams with thickness $T_{C,nd}=0.05L$ in every cell (Fig. 2c); and Design D, with no diagonal reinforcement and horizontal and vertical elements with thickness $T_{D,nd}=0.1L(1+1/\sqrt{2})$ (Fig. 2d). Note that in an effort to further provide a fair comparison, the volume ratio of diagonal to non-diagonal struts was also identical for Designs A, B and C (see Supplementary Section 2 and Supplementary Figs. 2–5 for details and assumptions).

We began our analysis by comparing the mechanical response under uniaxial compression along the vertical elements of the four lattices described above. Samples comprising 6×6 tessellations of

[1]John A. Paulson School of Engineering and Applied Sciences, Harvard University, Cambridge, MA, USA. [2]Wyss Institute, Harvard University, Cambridge, MA, USA. [3]Kavli Institute, Harvard University, Cambridge, MA, USA. ✉e-mail: jweaver@seas.harvard.edu; bertoldi@seas.harvard.edu

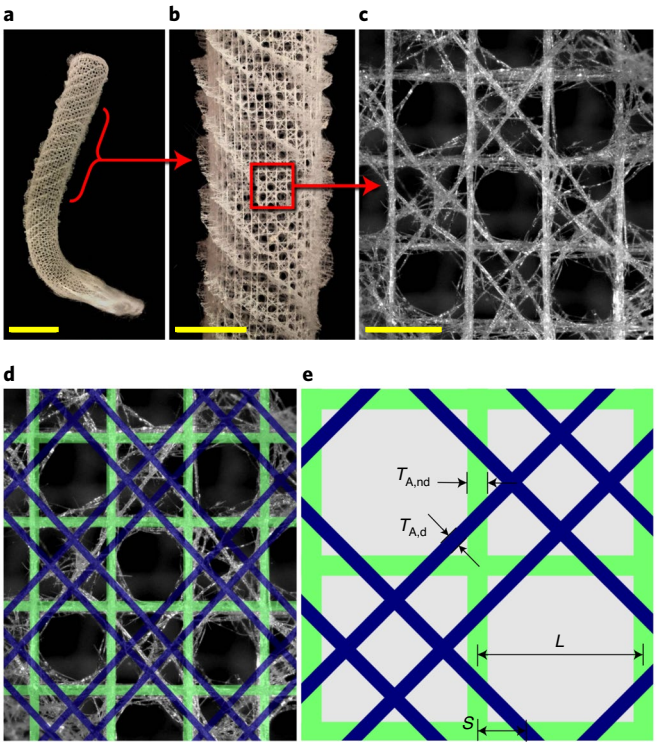

Fig. 1 | Representative skeletal system of the hexactinellid sponge *Euplectella aspergillum*. **a**–**c**, Progressively magnified views of the sponge's skeletal system, showing the entire skeletal tube (**a**), a magnified view of its highly regular lattice-like organization (**b**), and its alternating arrangemnet of open and closed cells (**c**). Scale bars, 4 cm (**a**); 2 cm (**b**); 2.5 mm (**c**). **d**, Composite overlay of an idealized truss model (green lines designate the vertical and horizonal truss elements, and the blue lines designate the diagonal truss elements) on the sponge's underlying skeletal structure. **e**, Schematic of Design A, comprising non-diagonal elements with length L and thickness $T_{A,nd}$ and diagonal elements with thickness $T_{A,d}$ located at a distance S from the nodes.

square cells with $L = 1.5$ cm and $H = 4$ cm were fabricated with a Connex500 multi-material 3D printer (Stratasys) from a Shore A 95 durometer material (digital elastomer FLX9795-DM) and compressed uniaxially using a single axis Instron (Model 5969) with a 50 kN load cell (Fig. 2e). Two key features emerged from the stress–strain curves reported in Fig. 2f. First, we found that all designs with diagonal reinforcement (that is, Designs A–C) were characterized by a nearly identical initial elastic response, demonstrating that the different diagonal reinforcement designs did not impact the structure's initial overall stiffness. Design D, as expected, exhibited a higher initial stiffness because of its thicker vertical and horizontal elements. Second, all curves showed a clear maximum load-bearing capacity, with Design A (the sponge-inspired design) accommodating the highest load. As each maximum load corresponded to the onset of buckling, we inferred that Design A displayed the highest critical buckling stress of the considered designs. Furthermore, we found that in all three designs with diagonals, the post-buckling behaviour resulted in a homogeneous pattern transformation throughout the sample (Fig. 2e). In contrast, for Design D, the critical mode resulted in a much larger wavelength than the size of a square unit cell, leading to a post-buckled shape qualitatively similar to that of a compressed buckled beam (more information on the experimental methods can be found in Supplementary Section 3 and Supplementary Table 1).

In an effort to understand how the sponge-inspired lattice design resulted in substantially improved mechanical performance, we conducted finite element simulations using ABAQUS/Standard (Dassault Systémes SE). For these analyses, the geometries were constructed using Timoshenko beam elements (ABAQUS element type B22) and the material's response was captured using an incompressible Neo-Hookean material model with a shear modulus $\mu = 14.5$ MPa. Our simulations consisted of three steps: (1) a buckling analysis (*BUCKLE step in ABAQUS) was conducted to obtain the buckling modes for each of the structures, (2) a perturbation in the form of the lowest buckling mode was then applied to the nodes of the mesh, and (3) a static nonlinear analysis (*STATIC step in ABAQUS) was performed to evaluate the nonlinear, large-deformation responses. To verify the validity of our

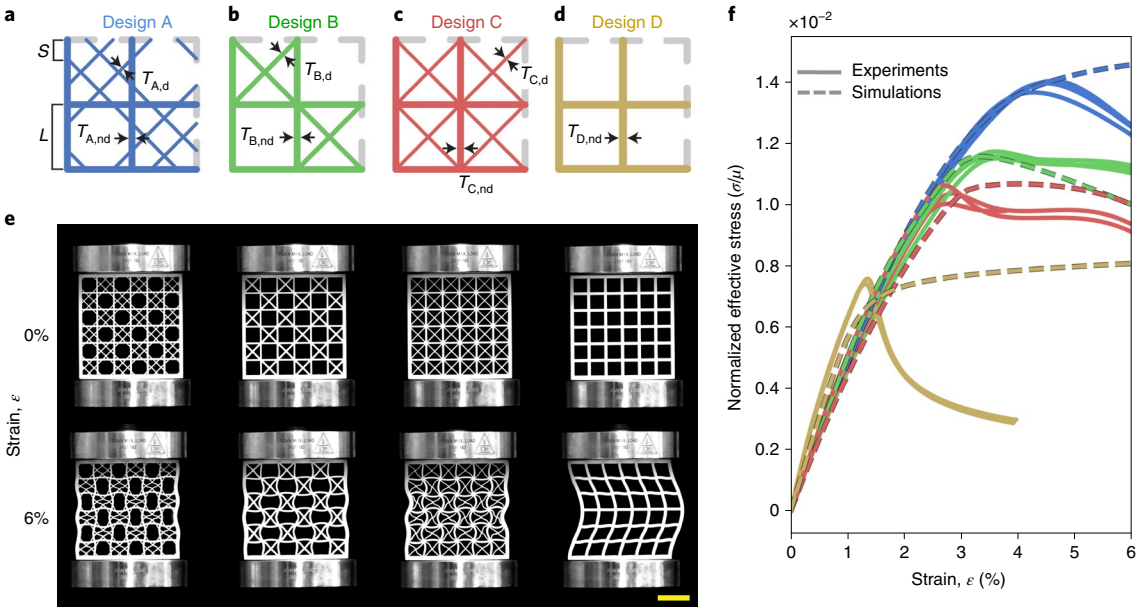

Fig. 2 | Experimental and numerical results. **a**–**d**, Schematics of designs A–D, respectively. **e**, Mechanical deformation snapshots of the different 3D-printed models at 0% applied strain (top) and 6% applied strain (bottom). Scale bar, 3 cm. **f**, Simulated and normalized experimental stress–strain curves for $n = 3$ independently tested samples of each design. Curves in this plot are colour coded according to **a**–**d**. All designs are characterized by the same total volume and mass ratio allocation between non-diagonal and diagonal elements.

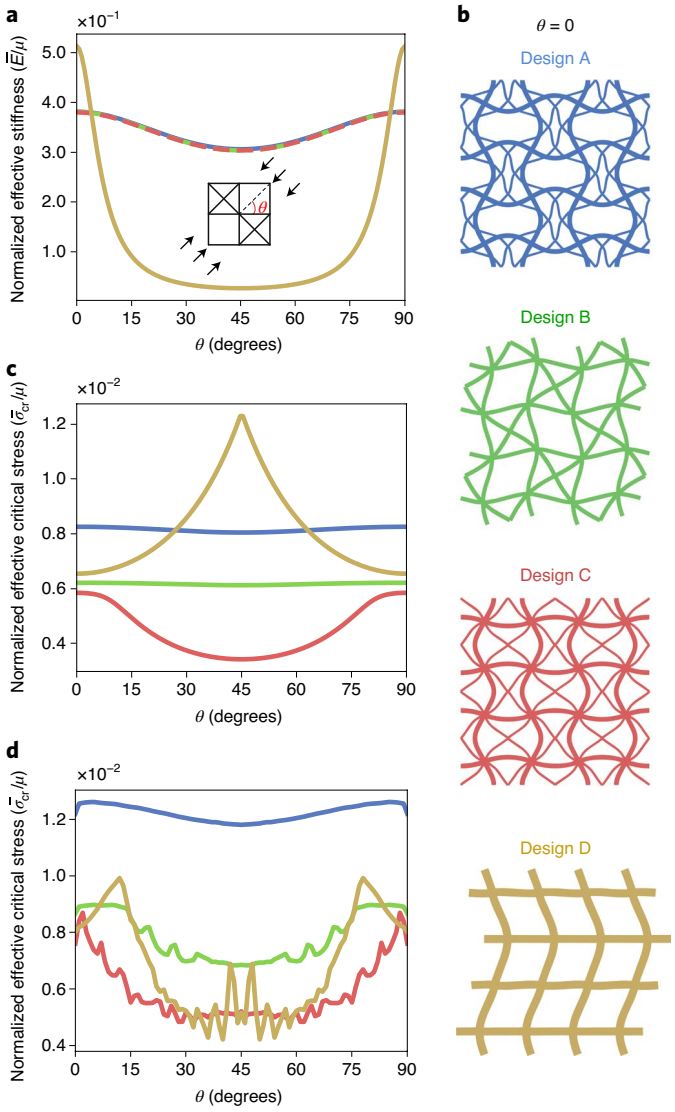

Fig. 3 | Numerical results describing structural response to varying loading angle. a, Evolution of the normalized structural stiffness for infinite size periodic lattice designs as a function of θ. **b**, Normalized critical buckling modes for Designs A–D at $\theta = 0°$. **c**, Evolution of the effective buckling stress for the different lattice designs as a function of θ. Results are obtained by simulating a supercell with 10×10 RVEs and periodic boundary conditions. **d**, Evolution of the normalized effective buckling stress as a function of θ for finite (non-periodic) lattice structures comprising 10×10 RVEs. In each plot, the line colour corresponds to the designs in **b**. All designs are characterized by the same total volume and mass ratio allocation between non-diagonal and diagonal elements.

analyses, we investigated the responses of models identical to those specimens tested in our Instron compression studies. As shown in Fig. 2f, we found close agreement between the numerical and experimental results up to the onset of buckling, confirming the accuracy of our simulations in capturing the linear regime and critical load. Next, we extended our finite element model to explore the effects of loading direction. To reduce computational cost and eliminate edge effects, we capitalized on the periodicity of the structures and investigated the response of representative volume elements (RVEs) with suitable periodic boundary conditions[16,17] (see Supplementary Section 4 and Supplementary Figs. 6–24 for details and additional numerical analysis). Figure 3a shows the evolution of the structures' effective stiffness, $\bar{E}$, as a function of the loading angle θ. We found that the stiffness of all structures containing diagonal reinforcement was virtually identical for any loading angle, further confirming that the structural stiffness was predominantly governed by the amount of material allocated along the loading direction. As a result, Design D, in which all of the material was allocated to the non-diagonal elements, exhibited the highest stiffness for $\theta = 0°$, but had almost negligible load-bearing capacity for $\theta = 45°$, where the only contribution to its stiffness came from the minimal bending resistance of the joints (see Supplementary Fig. 21 for a detailed analysis of the effect of joint stiffness).

Next, we investigated the effect of θ on the buckling behaviour of Designs A–D. We found that the effective critical buckling stress ($\bar{\sigma}_{cr}$) of Design A was higher than the other diagonally reinforced designs (Design B and Design C) for all values of θ (Fig. 3b). Design D surpassed Design A for $27° < \theta < 63°$ when considering an infinite structure. However, given the global nature of the buckling mode for Design D, such performance was largely affected by boundary effects and the critical buckling stress was substantially reduced when considering a finite size structure comprising 10×10 RVEs (Fig. 3d; see also Supplementary Fig. 20). Furthermore, the geometry of Design A maintained its robustness even after modifications to the lattice through the introduction of various levels of disorder, an observation consistent with the features observed in the native sponge skeleton (see Supplementary Figs. 23 and 24).

Having demonstrated the benefits of the sponge-inspired design (Design A) compared with Designs B–D, we wondered whether a different diagonally reinforced square lattice design with even higher critical buckling stress exists. To address this question, we formulated an optimization problem to identify the number of diagonals, N, their distance from the nodes of the square lattice S_i (where $i = 1, 2, \ldots, N$), as well as the ratio between diagonal and non-diagonal elements $\lambda = V_{nd}/V_d$ (V_{nd} and V_d being the volume of the non-diagonal and diagonal elements, respectively) that resulted in the highest buckling stress. Specifically, we considered finite size structures composed of 3×3 RVEs and focused on uniaxial compression parallel to the non-diagonal elements (that is, $\theta = 0°$), while constraining the total volume of the RVE to match that of the designs considered in Fig. 2. We maximized the objective function $\mathcal{Z} = \bar{\sigma}_{cr}$ using finite element simulations coupled to a Python implementation of the Covariance Matrix Adaptation Evolution Strategy algorithm (CMA-ES)[18] (more information on the implementation see Supplementary Section 5, Supplementary Figs. 25–27 and Supplementary Tables 2 and 3). For each set of inputs identified by CMA-ES, a finite element buckling analysis was conducted to obtain $\bar{\sigma}_{cr}$, which was subsequently used to evaluate the objective function $\mathcal{Z}$. We conducted seven separate optimizations, each considering a fixed integer number of diagonal elements N ranging from one to seven ($N = \mathbb{Z} \in [1, 7]$). Given the high strength of lattices reinforced by diagonals aligned at a 45° angle[19], we assumed in all of the runs that all of the diagonals were oriented at 45° with respect to the non-diagonal members and that V_d and V_{nd} were distributed equally among the diagonal and non-diagonal elements, respectively. Furthermore, to ensure symmetry, we assumed that $S_{2i-1} = S_{2i}$ ($i = 1, 2, \ldots, N/2$) if N is an even number and $S_1 = 0$ and $S_{2i-1} = S_{2i}$ ($i = 2, 3, \ldots, (N-1)/2$) for odd values of N. In Fig. 4a, we report the highest $\bar{\sigma}_{cr}$ identified by CMA-ES for all considered values of N. We found that the highest $\bar{\sigma}_{cr}$ was only 9.55% higher than that of Design A and occurred in a design similar to the sponge-inspired one (with two diagonals located at a distance $S = 0.1800L$ from the nodes, and volume distributed so that $\lambda = 0.6778$). As such, this numerical prediction, which was validated by experimental results (Fig. 4b), demonstrated that the sponge-inspired design was extremely close to the design that exhibited the highest critical stress.

Thus far, we demonstrated that the skeletal organization pattern found in *E. aspergillum* could be adapted to realize lattice

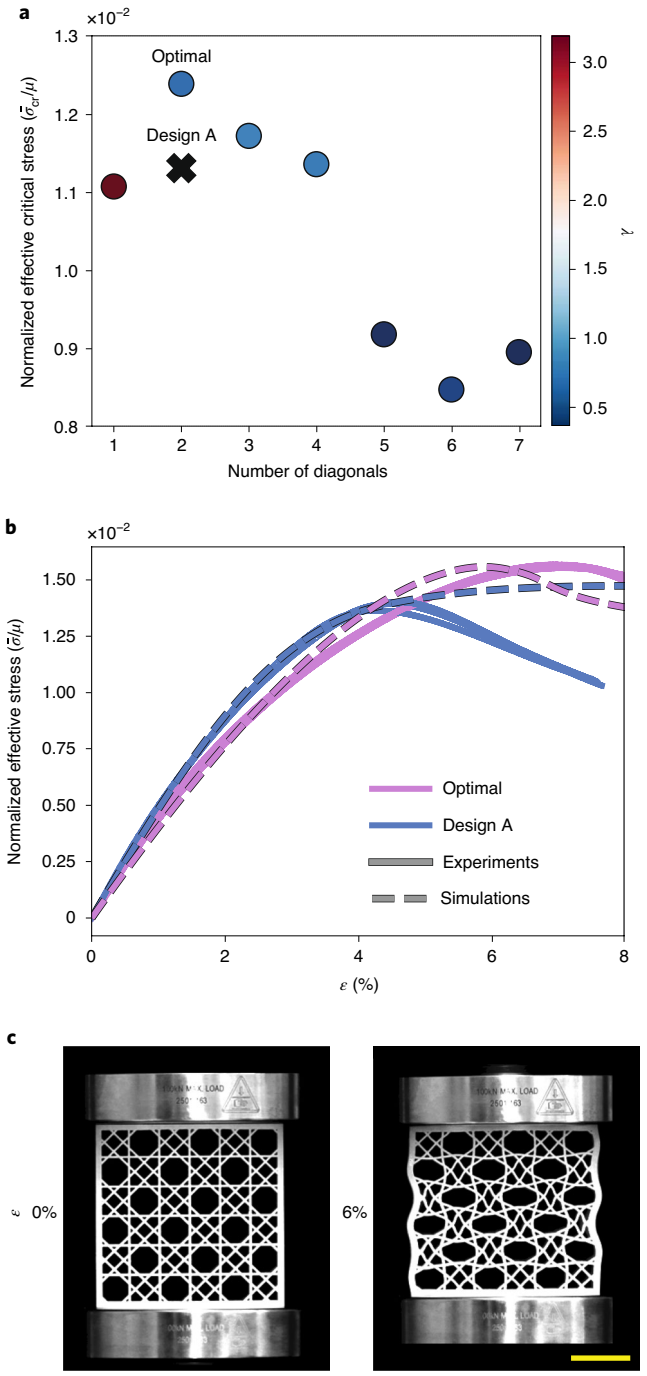

Fig. 4 | Optimization results and experimental validation. a, Optimal value of critical buckling load for varying numbers of diagonals. The colour of each point represents the optimal mass ratio λ. **b**, Simulated and normalized experimental stress–strain curves for $n=3$ independently tested samples of Design A and the optimal lattice design. **c**, Experimental snapshots of the optimal design at 0% applied strain (left) and 6% applied strain (right). Scale bar, 3 cm.

structures with high buckling resistance under uniaxial compression. However, it should be noted that the superior mechanical performance of the sponge-inspired lattice (Design A) is not limited to this loading condition. To demonstrate this important point, Fig. 5 shows results for a slender tessellation of 11×2 square cells loaded in three-point bending. In this scenario, using an Instron, the slender geometry was mounted in a three-point bending configuration and a displacement δ_{appl} was applied at the top centre of the geometry. As the displacement was applied, the reaction force was measured and plotted in Fig. 5b for the various geometries. Both our experiments and finite element simulations demonstrated that the sponge-inspired design was stiffer and could withstand 15% higher loads over a larger range of applied displacements, illustrating the potential benefit of incorporating such a design into suspended structures. We further used finite element simulations to evaluate the performance of Designs A–D in five other loading regimes. For all of the loading cases considered (see Supplementary Figs. 9–12), we found that Design A was able to withstand considerably higher loads than any of the other structures—making it the best candidate to realize load-bearing structures for a variety of applications. Although we focused on lattices at the centimetre scale in this study, we want to emphasize that our approach can be extended to design structures over a wide range of length scales as long as they lie within the continuum limit. However, in our analysis, we did not account for the effect of gravity, which could become a important source of loading for large-scale structures.

In summary, through analysis of the skeletal organization of *E. aspergillum*, we discovered that its non-trivial, double-diagonal, chequerboard-like square lattice design provides enhanced mechanical performance compared to existing structures. We compared the sponge-inspired lattice (Design A) to other common diagonally reinforced square lattices (Designs B and C) and a non-diagonally reinforced lattice (Design D), all with the same total mass, and found that the sponge-inspired design provides a superior mechanism for withstanding loads before the onset of buckling for a wide range of loading conditions. By using optimization tools to survey a broad multidimensional design space, we also found that the architecture of the sponge skeleton is nearly identical to the lattice design that provides the highest critical stress under uniaxial compression.

The results presented here therefore demonstrate that, by intelligently allocating material within a square lattice, it is possible to produce structures with optimal buckling resistance without the need to add more material to the system. The mechanical properties of the sponge-inspired lattice described here thus have implications for improving the performance of a wide range of truss systems, with applications ranging from large-scale infrastructure such as bridges and buildings to small-scale medical implants.

Although not the primary focus of this study, the results presented here may also shed light on functional aspects of the skeletal organization in *E. aspergillum*. It is important to note that skeletal maturation in this and related species progresses through two distinct phases (a flexible phase and a rigid phase), ultimately resulting in the terminal growth form shown in Fig. 1 (refs. [1,20,21]). In the early, flexible stage of growth, the vertical, horizontal and diagonal skeletal struts are not fused to one another, and can thus accommodate radial expansion of the skeletal cylinder. At this point, the mechanical behaviour of the sponge skeleton is dominated by the properties of the individual spicules, which have been reported to support large bending deformation and fail at strains greater than those found for buckling in our lattices—namely at strains greater than $\epsilon\approx0.04$ (refs. [22,23]). Once the maximum length and width of the cylindrical lattice is achieved, the skeleton goes through a series of rigidification steps, resulting in a progressive stiffening of the skeletal system through nodal fusion of the vertical, horizontal and diagonal struts via the deposition of a lower-modulus laminated silica cement[24], followed by the addition of the spiralling external ridges and further densification of the skeleton. Therefore, although the results presented here are thus unlikely to be biologically relevant with regards to the fully mature skeleton shown in Fig. 1, they may very well be relevant during the early stages of skeletal consolidation in this and related species where the buckling strains exceed the laminate yield strains[22–24].

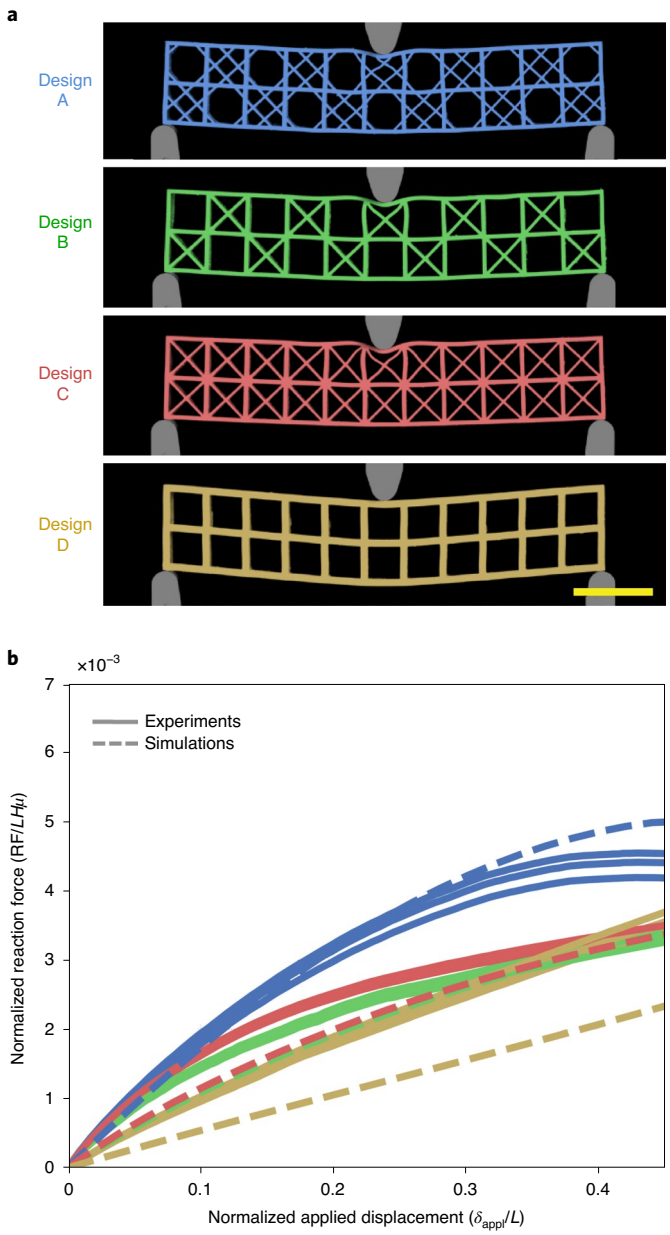

Fig. 5 | Numerical and experimental results of slender structures undergoing 3-point bending tests. a, Experimental snapshots of the four lattices comprising 11 × 2 square cells when loaded in three-point bending at $\delta_{appl}/L = 0.45$. Scale bar, 3 cm. The photographs have been false-coloured to more clearly reflect the corresponding plots in **b** for each design. **b**, Evolution of the normalized reaction forces for $n = 3$ experimentally obtained samples (solid lines) and simulations (dashed lines) of the four designs as a function of the applied displacement. Normalization involved dividing the resulting reaction forces by the material shear modulus, specimen cell length L, and specimen depth H.

Online content

Any methods, additional references, Nature Research reporting summaries, source data, extended data, supplementary information, acknowledgements, peer review information; details of author contributions and competing interests; and statements of data and code availability are available at https://doi.org/10.1038/s41563-020-0798-1.

Received: 12 December 2019; Accepted: 11 August 2020;
Published online: 21 September 2020

References

1. Schulze, F. E. Report on the hexactinellida collected by H.M.S. *Challenger* during the years 1873–76. In *Report on the Scientific Results of the Voyage of H.M.S. Challenger During the Years 1873–76* (eds Thomson, C. W. & Murray, J.) *Zoology* Vol. 21, 1–513 (Neill and Co., 1887).
2. Aizenberg, J. et al. Skeleton of *Euplectella* sp.: structural hierarchy from the nanoscale to the macroscale. *Science* **309**, 275–278 (2005).
3. Weaver, J. C. et al. Unifying design strategies in demosponge and hexactinellid skeletal systems. *J. Adhes.* **86**, 72–95 (2010).
4. Miserez, A. et al. Effects of laminate architecture on fracture resistance of sponge biosilica: lessons from nature. *Adv. Funct. Mater.* **18**, 1241–1248 (2008).
5. Monn, M. A., Weaver, J. C., Zhang, T., Aizenberg, J. & Kesari, H. New functional insights into the internal architecture of the laminated anchor spicules of *Euplectella aspergillum*. *Proc. Natl Acad. Sci. USA* **112**, 4976–4981 (2015).
6. Schaedler, T. A. et al. Ultralight metallic microlattices. *Science* **334**, 962–965 (2011).
7. Ashby, M. F. The properties of foams and lattices. *Phil. Trans. R. Soc. Lond. A* **364**, 15–30 (2006).
8. Evans, A. G., Hutchinson, J. W., Fleck, N. A., Ashby, M. F. & Wadley, H. N. G. The topological design of multifunctional cellular metals. *Prog. Mater. Sci.* **46**, 309–327 (2001).
9. Phani, A. S., Woodhouse, J. & Fleck, N. A. Wave propagation in two-dimensional periodic lattices. *J. Acoust. Soc. Am.* **119**, 1995–2005 (2006).
10. Lu, T. J., Stone, H. A. & Ashby, M. F. Heat transfer in open-cell metal foams. *Acta Mater.* **46**, 3619–3635 (1998).
11. Ashby, M. F., Seymour, C. J. & Cebon, D. *Metal Foams and Honeycombs Database* (Granta Design, 1997).
12. Evans, A. G., Hutchinson, J. W. & Ashby, M. F. Multifunctionality of cellular metal systems. *Prog. Mater. Sci.* **43**, 171–221 (1998).
13. Deshpande, V. S., Ashby, M. F. & Fleck, N. A. Foam topology: bending versus stretching dominated architectures. *Acta Mater.* **49**, 1035–1040 (2001).
14. Gibson, L. J. & Ashby, M. F. *Cellular Solids: Structure and Properties* (Cambridge Univ. Press, 1999).
15. Phani, A. S. & Hussein, M. I. *Dynamics of Lattice Materials* (John Wiley & Sons, 2017).
16. Danielsson, M., Parks, D. M. & Boyce, M. C. Three-dimensional micromechanical modeling of voided polymeric materials. *J. Mech. Phys. Solids* **50**, 351–379 (2002).
17. Bertoldi, K. & Boyce, M. C. Mechanically triggered transformations of phononic band gaps in periodic elastomeric structures. *Phys. Rev. B* **77**, 052105 (2008).
18. Hansen, N., Akimoto, Y. & Baudis, P. CMA-ES/pycma: r3.0.3. https://doi.org/10.5281/zenodo.2559634 (2019).
19. Horne, M. R. & Merchant, W. *The Stability of Frames* (Elsevier, 1965).
20. Schulze, F. E. Hexactinellida. In *Scientific Results of the German Deep-Sea Expedition with the Steamboat, Valdivia 1898–1899* (ed. Chun, C.) (Gustav Fischer, 1904).
21. Saito, T., Uchida, I. & Takeda, M. Skeletal growth of the deep-sea hexactinellid sponge *Euplectella oweni*, and host selection by the symbiotic shrimp *Spongicola japonica* (crustacea: Decapoda: Spongicolidae). *J. Zool.* **258**, 521–529 (2002).
22. Walter, S. L., Flinn, B. D. & Mayer, G. Mechanisms of toughening of a natural rigid composite. *Mater. Sci. Eng. C* **27**, 570–574 (2007).
23. Monn, M. A., Vijaykumar, K., Kochiyama, S. & Kesari, H. Lamellar architectures in stiff biomaterials may not always be templates for enhancing toughness in composites. *Nat. Commun.* **11**, 373 (2020).
24. Woesz, A. et al. Micromechanical properties of biological silica in skeletons of deep-sea sponges. *J. Mater. Res.* **21**, 2068–2078 (2006).

Methods

Parameter derivation and an explanation of each geometry can be found in Supplementary Section 2. Details of the fabrication of the samples and the protocol for testing can be found in Supplementary Section 3. The numerical set-up and explanation for the finite element analysis can be found in Supplementary Section 4. Additional numerical analysis, including parameter exploration and considerations for different cross-sectional geometries, is presented in Supplementary Section 4.1. A detailed description of the optimization algorithm can be found in Supplementary Section 5.

Data availability

Raw data for the plots are available on GitHub at http://fer.me/sponge-structure. Additional data that support the findings of this study are available from the corresponding authors on request.

Code availability

All codes necessary to reproduce results in main paper are available on GitHub at http://fer.me/sponge-structure.

Acknowledgements

This work was supported by NSF-GRFP Fellowship Grant Number DGE-1144152 (M.C.F.), a GEM Consortium Fellowship (M.C.F.) and the Harvard Graduate Prize Fellowship (M.C.F.), and was partially supported by the NSF through the Harvard University Materials Research Science and Engineering Center Grant Number DMR-2011754 and NSF DMREF Grant Number DMR-1922321. We also thank J. R. Rice, J. W. Hutchinson, F. H. Abernathy, J. Vlassak, S. Gerasimidis and C. Rycroft for discussions.

Author contributions

All authors secured research funding. K.B. and J.C.W. supervised the research. M.C.F. and J.C.W. generated models and performed mechanical testing and finite element simulations. M.C.F., K.B. and J.C.W. analysed the data. All authors wrote the paper.

Competing interests

The authors would like to disclose a submitted patent application on related geometric features reported in this manuscript. United States Patent and Trademark Office (USPTO) (RO/US) application number: 002806-094100WOPT filed in 2019. Patent applicant: President and Fellows of Harvard College. Inventors: Matheus C. Fernandes, James C. Weaver, and Katia Bertoldi. The authors declare no further competing interests.

Additional information

Supplementary information is available for this paper at https://doi.org/10.1038/s41563-020-0798-1.

Correspondence and requests for materials should be addressed to J.C.W. or K.B.